Supplementary Information (SI) for Journal of Materials Chemistry A.

Supporting Information

Anode engineering using hybrid $AlCl_3$/PTHF coating for enhanced electrochemical stability of Mg–O_2 batteries

Vasantan Rasupillai Dharmaraj,[a,b] Ayan Sarkar,[a] Yueh-An Wu,[a] Han-Chen Chen,[c] Yu-Ping Lin,[c] Ren-Jei Chung,[b] and Ru-Shi Liu*[a]*

[a]Department of Chemistry and the Advanced Research Center for Green Materials Science and Technology, National Taiwan University, Taipei 106, Taiwan.

[b]Department of Chemical Engineering and Biotechnology, National Taipei University of Technology, Taipei 106, Taiwan.

[c]Dexin Advanced Technology Co., Hsinchu 302, Taiwan

Corresponding authors

rjchung@ntut.edu.tw (R. J. Chung), rsliu@ntu.edu.tw (R. S. Liu)

1. Materials and reagents

Poly(vinylidene fluoride-co-hexafluoropropylene) (PVDF-HFP; $(-CH_2-CF_2-)_x-[-CF_2-CF(CF_3)-]y$, average molecular weight (Mw) ~400,000, 99% pure, Sigma–Aldrich), N,N-dimethylacetamide (≥99% pure, Acros Organics), acetone (99.5% pure, Fisher Scientific), 1-butyl-1-methylpyrrolidinium N,N-bis[(trifluoromethyl)sulfonyl]amide ($Pyr_{14}TFSI$; 99% pure, Uni Region), magnesium nitrate hexahydrate ($Mg(NO_3)_2·6H_2O$, 99% pure, Thermo Fisher Scientific), tetrahydrofuran (THF; 99.9985% pure, Acros Organics), aluminum chloride hexahydrate ($AlCl_3·6H_2O$; 99.8% pure, Merck), diethylene glycol dimethyl ether (Diglyme, 99% pure, Alfa Aesar), and magnesium metal as anode (Shinning Energy Company Ltd., Hsinchu, Taiwan) with a thickness of 0.05 mm after polishing were used in this study.

2. Electrolyte synthesis

The quasi-solid-state electrolyte was prepared by synthesizing a PVDF-HFP membrane through electrospinning. A 16 wt% PVDF-HFP solution was dissolved in a solvent mixture containing acetone and N, N-dimethylacetamide (7:3 v/v). The solution was electrospun under optimized conditions, including a 22 kV voltage, a 0.5 mL h^{-1} flow rate, and a 15 cm needle-to-collector distance, yielding a uniform fibrous membrane. The resultant membrane was vacuum-dried at 50 °C for 12 h. A binary liquid electrolyte was prepared using a 1:1 molar ratio of magnesium nitrate hexahydrate ($Mg(NO_3)_2·6H_2O$) and $Pyr_{14}TFSI$ dissolved in diethylene glycol dimethyl ether (diglyme). The liquid electrolyte was infused into the electrospun membrane by dropwise addition (10 μL), and the composite was vacuum dried at 60 °C for 24 h to eliminate residual solvents. The prepared electrospun electrolyte was used as the separator in all electrochemical tests for the $Mg–O_2$ battery (MOB) system.

3. Cathode synthesis

Ru/CNT catalytic cathodes were synthesized following established protocols with slight modifications. 36 mg of Ru/CNTs was combined with 4 mg of PVDF in NMP and subjected to ball milling at 3000 rpm for 1 h to create a homogeneous slurry suitable for battery applications. Approximately 10 µL of this slurry was uniformly drop-casted onto a carbon paper (1 cm radius) that had been pre-dried under vacuum. Subsequently, the coated cathodes were vacuum dried at 80 °C for 12 h to eliminate residual solvent and enhance structural stability, resulting in active material loadings ranging from 0.15 to 0.25 mg per cell. Furthermore, the cathode was used along with the electrospun electrolyte (1:1 M) to form a sandwich design, which promotes excellent Mg^{2+} ion migration.

4. Electroanalytical techniques

Electrochemical tests of Magensium-Oxygen batteries (MOBs) at room temperature were performed using a battery tester from AcuTech Systems Co., Ltd., Taiwan. The cycling capabilities of the MOBs were evaluated at a current density of 100 mA g^{-1}, achieving a limiting capacity of 500 mAh g^{-1} within a voltage range of 0.5–3.5 V (vs. $Mg^{2+/}Mg$). The specific capacity was determined using the total mass of the active ingredient. Electrochemical impedance (0.1 Hz to 10^7 Hz at an open circuit potential with a 10 mV AC perturbation), chronoamperometry measurement, Tafel plot measurement data of pristine and modified Mg anodes and electrospun electrolytes were recorded using the Autolab ECI10M model instrument.

5. Characterization techniques

The room-temperature powder X-ray diffraction patterns of the anode samples were recorded using the Cu Kα line (λ = 1.54178 Å) equipped with a Bruker D2 PHASER instrument. Fourier transform infrared (FT-IR) spectra were obtained using a PerkinElmer Spectrum Two FT-IR Spectrometer (L160000F) in attenuated total reflectance mode. The morphology and energy-dispersive X-ray spectroscopy (EDS) of bare anode, modified anode, and maximum discharged cathodes were examined using field emission scanning electron microscopy (FESEM, Hitachi Regulus-8100). Relevant X-ray photoelectron spectra were obtained using Micromeritics

ASAP2020 ASAP2010 and a Thermo Scientific Theta Probe (113R, 20085). A JEOL JSM-7600F system was used for transmission electron microscopy (TEM), high-resolution TEM (HRTEM), and selected area electron diffraction equipped with an OXFORD X-MaxN TSR EDS mapping instrument for the pristine Ru/CNT and maximum-discharged cathode.

6. Additional characterizations

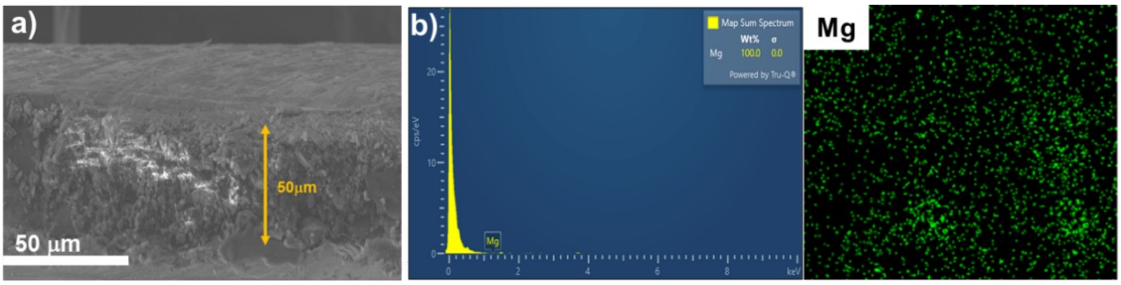

Figure S1. FE-SEM (a) cross-sectional micrograph of pristine Mg metal with corresponding (b) EDS spectrum and elemental color map.

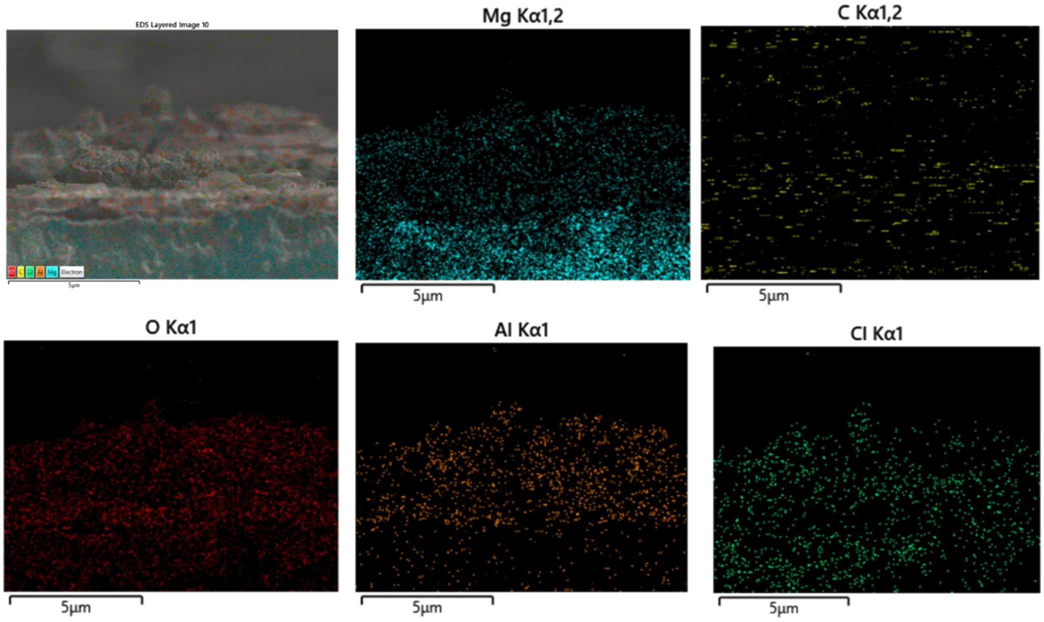

Figure S2. EDS elemental color mappings of the unused, modified Mg anode cross-section.

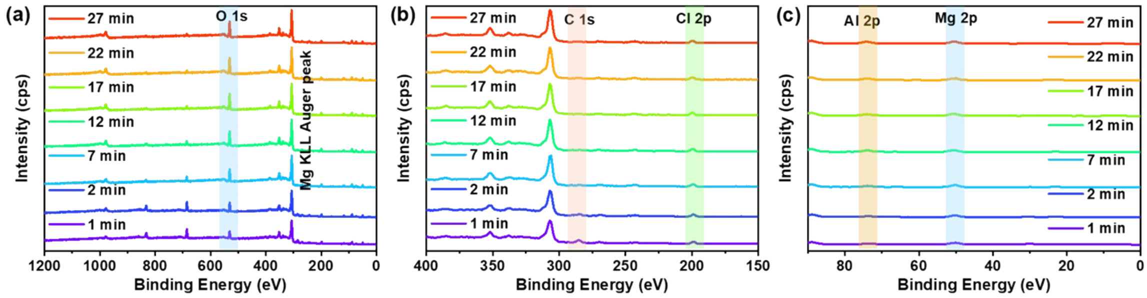

Figure S3. (a) XPS full survey spectra of the SEI layer on the Mg anode at different Ar$^+$-ion irradiation (3 kV) times. XPS narrow scan spectra showing the binding energy region from (b) 150 to 400 eV and (c) 90 to 0 V for the SEI layer on the Mg anode.

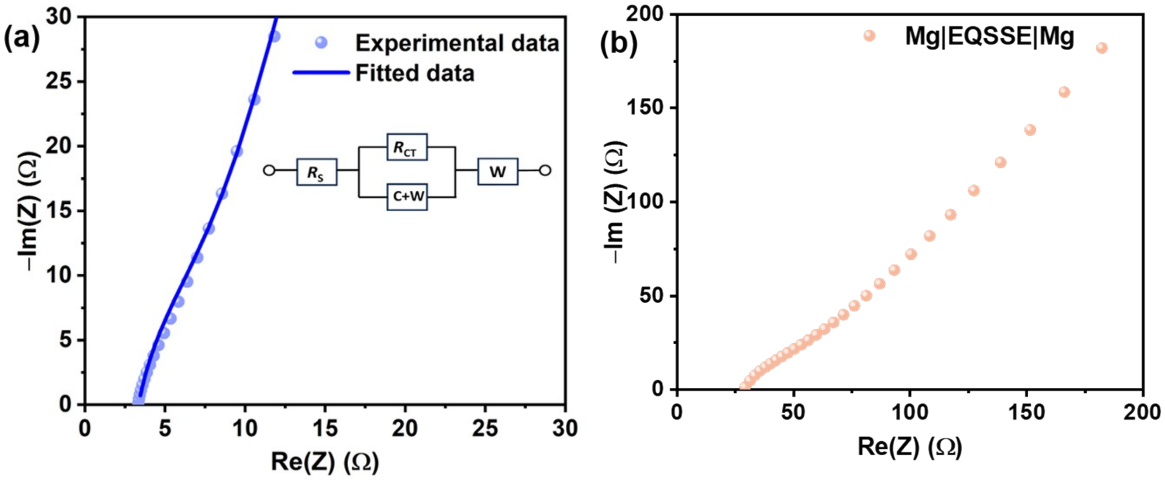

Figure S4. (a) Nyquist plot of the EQSSE-based electrolyte for measuring conductivity. (b) Nyquist plot of EQSSE-based gel electrolyte with unmodified Mg anodes at both sides.

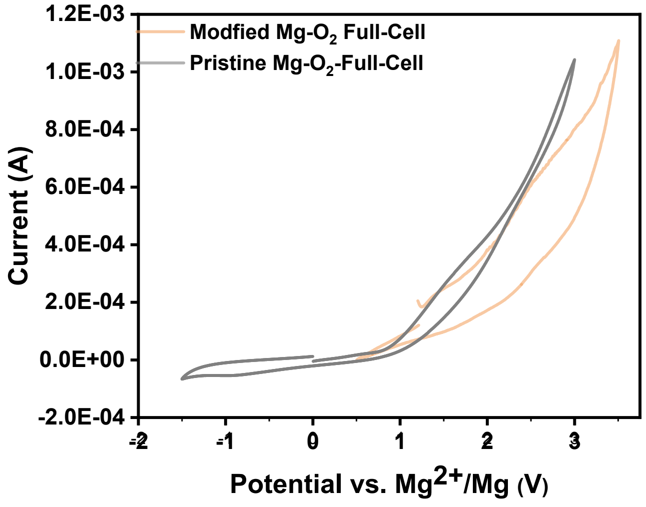

Figure S5. Cyclic voltammetry of pristine and modified Mg anode.

Figure S5 illustrates the cyclic voltammetry (CV) profiles of MOBs with pristine and $AlCl_3$/PTHF-modified Mg anodes. The modified Mg anode exhibits an open-circuit voltage of ~1.1 V, an oxygen reduction (ORR) peak at ~1.3 V, and an oxidation evolution reaction (OER) peak at ~2.4 V, indicating a stable and reversible ORR/OER facilitated by the hybrid solid electrolyte interphase (SEI) layer. By contrast, the pristine Mg anode shows broader peaks with high overpotentials (ORR, ~1.4 V; OER, ~2.6 V) and poor interfacial stability. The reduced overpotential (~1.1 V) and enhanced electrochemical kinetics of the modified anode indicate that $AlCl_3$/PTHF coating plays an important role in ensuring consistent Mg^{2+} ion transport and mitigating parasitic reactions, thereby highlighting its potential for efficient and durable MOB applications.

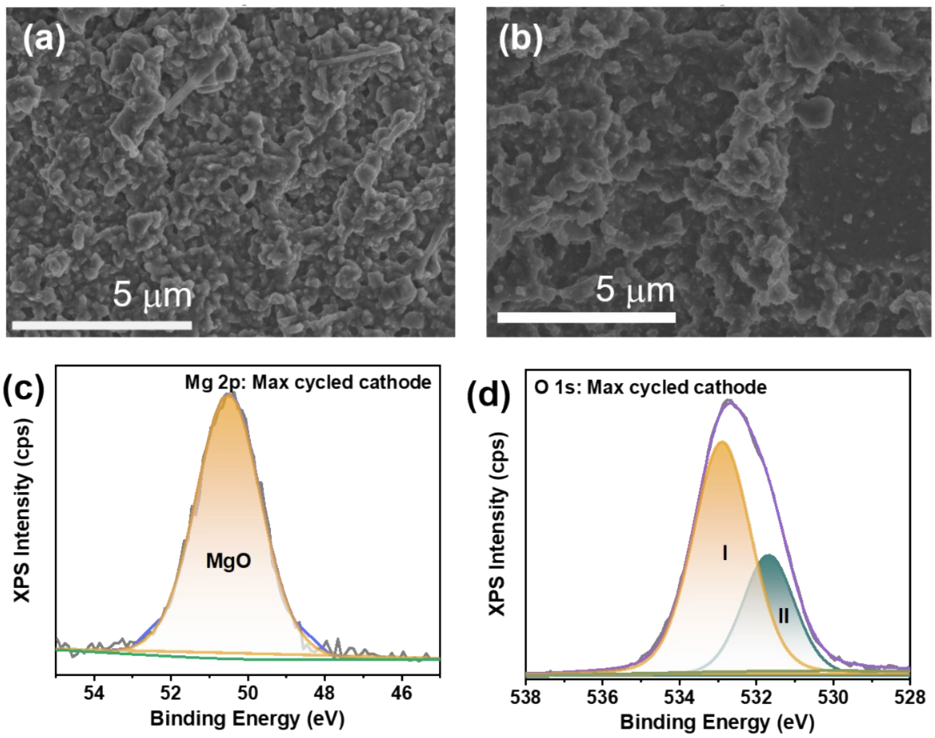

Figure S6. FESEM micrographs of the Ru/CNT cathodes after (a) maximum discharge and (b) maximum GDC cycling. Deconvoluted XPS spectra of (a) Mg 2p and (b) O 1s for the Ru/CNT cathode post-cycling. Peaks at 530.8 eV (MgO, Peak I) and 531.8 eV (residual electrolyte components, Peak II).

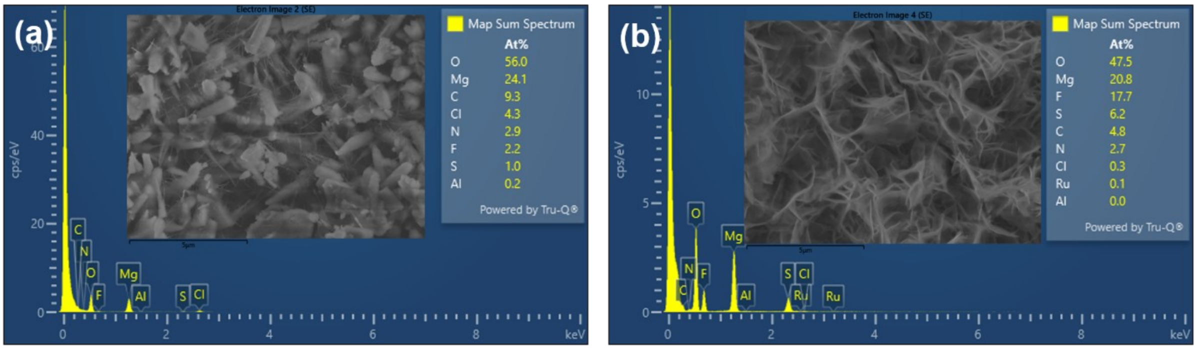

Figure S7. FESEM micrograph (inset) and the EDS spectrum of that area with atomic% of the constituent elements for the (a) modified anode of the Mg–O_2 battery after maximum galvanostatic discharge/charge cycles and (b) modified anode from the maximum discharged Mg–O_2 battery.

Table S1. The development of Mg–O_2 batteries over the years compared to this study.

Sl. No.	Cathode	Electrolytes	Anode	Cycle No.	Maximum discharge capacities [mAh g^{-1}]	References
1	Carbon Black	I_2-DMSO	Mg	4	2131	1
2	Carbon	$Mg(TFSA)_2$-DEMETFSA	Mg	3	737	2
3	Carbon Black	$(PhMgCl)_4$–$Al(OPh)_3$/THF	Mg	3	0.013	3
4	Carbon Paper	$Mg(TFSI)_2$/$Mg(ClO_4)_2$/TBAPF$_6$-DMSO	Mg	3	0.06	4
5	MnO_2	NaCl, $NaNO_3$, $NaPO_4$-NaCl/$NaPO_4$	Mg	3	10	5
6	Pt-C	$Mg(ClO_4)_2$/DMSO	Mg	3	380	6
7	RuO_2/Pt-C	$Mg(TFSI)_2$/diglyme	Bi@Mg	5	1000	7
8	Pt-C	$Mg(TFSI)_2$-$MgCl_2$/diglyme	Mg	35	1600	8
9	Ru/CNT	$Mg(TFSI)_2$/diglyme	Mg	27	25340	[9] (our group)
10	Ru/CNT	$Mg(NO_3)_2$-$Mg(TFSI)_2$/Diglyme	Mg	65	25793	[9] (our group)
11	Ru/CNT	PEO-SN-$Mg(OTf)_2$-$Mg(TFSI)_2$-G2	Mg	50	9489	[10] (our

						group)
12	Ru/CNT	PVDF-HFP-$Mg(NO_3)_2$-$Pyr_{14}TFSI$-G2	$AlCl_3$/PTHF-modified Mg	50	6184	This study

A note on the performances demonstrated in Sl. No. 9–12

It is important to clarify that while the maximum discharge capacities reported in References 9 and 10 were high, those systems involved significantly different cell configurations and electrolyte environments. Specifically, in Reference 9, we used a liquid electrolyte system (2 M $Mg(NO_3)_2$ and 1 M $Mg(TFSI)_2$ in diglyme), achieving a high discharge capacity of 25,793 mAh g^{-1} at 100 mA g^{-1}, but with a mid-term overpotential of ~1.4 V and only 65 galvanostatic discharge-charge (GDC) cycles. In Reference 10, we employed a PEO-SN-$Mg(OTf)_2$-based polymer electrolyte along with a $Mg(TFSI)_2$-G2 catholyte layer, achieving a maximum discharge capacity of ~9500 mAh g^{-1} and 51 GDC cycles at 100 mA g^{-1}, but with an average overpotential of ~1.14 V.

In contrast, the current work focuses on a quasi-solid-state-like configuration with an $AlCl_3$/PTHF-modified Mg anode, which enables significantly enhanced stability and lower overpotentials. We demonstrate over 300 h of stable symmetric cell operation (Figure 5(a)), and a notably reduced overpotential of ~0.9 V sustained over 50 cycles in a full cell (Figure 6(b)). This marks a substantial improvement in interfacial stability and Mg^{2+} transport behavior, even though the absolute capacity is somewhat lower.

Thus, while the earlier systems prioritized high capacity using liquid or semi-liquid catholyte additives, the current study prioritizes interfacial engineering for improved stability, suppressed overpotential, and practical feasibility in quasi-solid-state architectures. We believe this represents a significant advancement and complementary direction in developing stable and efficient Mg batteries.

References

1 T. Shiga, Y. Hase, Y. Kato, M. Inoue and K. Takechi, *Chem. Commun.*, 2013, **49**, 9152–9154.

2 T. Shiga, Y. Hase, Y. Yagi, N. Takahashi and K. Takechi, *J. Phys. Chem. Lett.*, 2014, **5**, 1648–1652.

3 G. Vardar, E. G. Nelson, J. G. Smith, J. Naruse, H. Hiramatsu, B. M. Bartlett, A. E. S. Sleightholme, D. J. Siegel and C. W. Monroe, *Chem. Mater.*, 2015, **27**, 7564–7568.

4 Q. Dong, X. Yao, J. Luo, X. Zhang, H. Hwang and D. Wang, *Chem. Commun.*, 2016, **52**, 13753–13756.

5 F. W. Richey, B. D. McCloskey and A. C. Luntz, *J. Electrochem. Soc.*, 2016, **163**, A958–A963.

6 P. Fischer, R. M. Schwarz, M. Marinaro, M. Wachtler and L. Jörissen, *ECS Trans.*, 2017, **75**, 3–12.

7 Y. Zhao, A. Du, S. Dong, F. Jiang, Z. Guo, X. Ge, X. Qu, X. Zhou and G. Cui, *ACS Energy Lett.*, 2021, **6**, 2594–2601.

8 K. L. Ng, K. Shu and G. Azimi, *iScience*, 2022, **25**, 104711.

9 V. Rasupillai Dharmaraj, A. Sarkar, C. H. Yi, K. Iputera, S. Y. Huang, R. J. Chung, S. F. Hu and R. S. Liu, *ACS Appl. Mater. Interfaces*, 2023, **15**, 9675–9684.

10 A. Sarkar, S. Y. Huang, V. Rasupillai Dharmaraj, B. Bazri, K. Iputera, H. H. Su, Y. A. Chen, H. C. Chen, Y. P. Lin, R. J. Chung, D. H. Wei and R. S. Liu, *J. Mater. Chem. A*,

2024, **12**, 25968–25978.